ACS APPLIED MATERIALS & INTERFACES

Research Article

Cite This: ACS Appl. Mater. Interfaces 2017, 9, 43113−43126

www.acsami.org

NIR Emitting Nanoprobes Based on Cyclic RGD Motif Conjugated PbS Quantum Dots for Integrin-Targeted Optical Bioimaging

N. Depalo,[*,†,○] M. Corricelli,[†,○] I. De Paola,[‡] G. Valente,[†] R. M. Iacobazzi,[§] E. Altamura,[∥] D. Debellis,[∥,▽] D. Comegna,[‡] E. Fanizza,[†,∥] N. Denora,[†,⊥] V. Laquintana,[⊥] F. Mavelli,[∥] M. Striccoli,[†] M. Saviano,[#] A. Agostiano,[†,∥] A. Del Gatto,[‡] L. Zaccaro,[‡] and M. L. Curri[*,†]

[†]Istituto per i Processi Chimico-Fisici-CNR SS Bari, Via Orabona 4, 70125 Bari, Italy

[‡]Istituto di Biostrutture e Bioimmagini-CNR, Via Mezzocannone 16, 80134 Napoli, Italy

[§]Istituto Tumori IRCCS Giovanni Paolo II, Viale Orazio Flacco 65, 70124 Bari, Italy

[∥]Dipartimento di Chimica and [⊥]Dipartimento di Farmacia-Scienze del Farmaco, Università degli Studi di Bari Aldo Moro, Via Orabona 4, 70125 Bari, Italy

[#]Istituto di Cristallografia-CNR Bari, Via Amendola 122/O, 70126 Bari, Italy

Supporting Information

ABSTRACT: Here, silica-coated PbS quantum dots (QDs) with photoluminescence emission properties in the near-infrared (NIR) region are proposed as potential effective single particle optical nanoprobes for future in vivo imaging of tumors. The dispersibility in aqueous medium of hydrophobic PbS QDs was accomplished by growing a silica shell on their surface by exploiting a base assisted water-in-oil microemulsion method. The silica-coated PbS QDs were then conjugated with a specifically designed cyclic arginine−glycine−aspartic acid (cRGD) peptide that is able to specifically recognize $\alpha v\beta 3$ integrins, which are overexpressed in angiogenic tumor-induced vasculatures and on some solid tumors, to achieve tumor-specific targeting. The cRGD peptide PbS silica-coated QDs were systematically characterized, at each step of their preparation, by means of complementary optical and structural techniques, demonstrating appropriate colloidal stability and the maintenance of their optical futures in aqueous solutions. The cellular uptake of cRGD peptide functionalized luminescent nanostructures in human melanoma cells, where overexpression of $\alpha v\beta 3$ was observed, was assessed by means of confocal microscopy analysis and cytometric study. The selectivity of the cRGD peptide PbS silica-coated QDs for the $\alpha v\beta 3$ integrin was established, consequently highlighting the significant potential of the developed NIR emitting nanostructures as optically traceable nanoprobes for future $\alpha v\beta 3$ integrin receptor in vivo targeting in the NIR region.

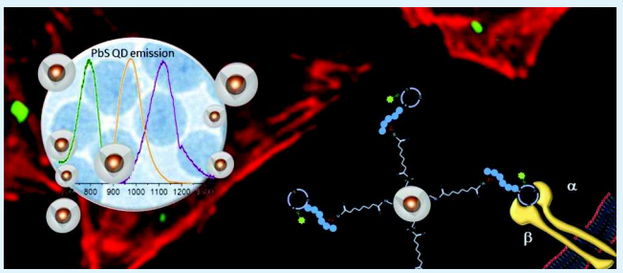

KEYWORDS: *NIR emitting quantum dots, silica-coated nanoprobes, cyclic RGD peptide, αvβ3 integrin receptor, targeted imaging*

1. INTRODUCTION

Targeted molecular imaging represents an efficient approach for the advanced diagnosis of cancer and for the real-time evaluation of the effects of therapies. Crucial for targeted molecular imaging are the design and realization of imaging probes, characterized by a high affinity to bind to the target sites, selective cellular internalization, and an in vivo high stability.[1] In addition, such probes are required to be safe and easy to prepare. In this perspective, the use of probes based on peptides was most effective in molecularly targeted imaging, thanks to the peculiar advantages of peptides when compared with other biological or small molecules.[2−6] Indeed, a wide range of peptide ligand receptors, i.e., somatostatin, integrin, neurotensin, and gastrin-releasing peptide, were recently identified, thus indicating them as potential targets for tumor receptor imaging.[7−13] Furthermore, peptides are characterized by a good tissue penetrating ability, along with a low immunogenicity and high affinity to targets. Interestingly, they can be easily conjugated with specific imaging agents suited for different imaging modalities.[14−16]

Indeed, various imaging agents, such as radiometals and fluorophores, have been combined with properly designed peptides for their use as in vivo traceable agents for diverse imaging techniques. For example, a wide range of radionuclides was coupled with specific peptides and exploited for positron emission tomography or single-photon-emission computed tomography. Similarly, peptide/paramagnetic agent or peptide/fluorescent dye-based probes were employed for magnetic

Received: September 18, 2017
Accepted: November 17, 2017
Published: November 17, 2017

DOI: 10.1021/acsami.7b14155
ACS Appl. Mater. Interfaces 2017, 9, 43113−43126

resonance imaging and optical imaging, respectively.[17−22] Compared to the plethora of imaging modalities, optical imaging allows numerous advantages to be obtained, including accurate sensitivity, noninvasivity, and its moderate cost of detection instrumentation. Interestingly, the use of fluorescent probes emitting in the near-infrared region (NIR, 700−1100 nm), or so-called biological transparent window, can in principle improve the signal-to-noise ratio in optical in vivo imaging. In the NIR region, autofluorescence and scattering by biological tissues are minimal, therefore NIR probes are expected to result in high resolution and deep penetration images. Despite continuous efforts in the synthesis of organic dyes active in this spectral region and characterized by higher brightness and stability,[23] nanoparticles (NPs), such as inorganic quantum dots (QDs) and metal or rare earth-based nanostructures and nanodiamonds, represent valuable alternative probes emitting in the NIR region.[24] Among them, NIR emitting inorganic QDs are characterized by tuneable emission properties depending on their size and composition, high brightness, due to their elevated quantum yields (QY), and improved photostability in comparison to organic molecular dyes.[25−27] In addition, the QD surface can be efficiently functionalized with a variety of targeting ligands or imaging molecules. A single nano-object based probe can be conveniently surface engineered by functionalization with different targeting and imaging agents, thus offering enhanced binding affinity and specificity, as well as an amplified optical response from the target region.[28−30] Furthermore, the use of targeted nanoplatform-based probes is expected to prolong plasma half-lives, thus enhancing their in vivo stability and targeting efficiency. Several examples of nontargeted QDs were proposed as efficacious fluorescent agents for visualization of trafficking inside cell and in vivo imaging. However, despite the potential of the nontargeted QD probes in the NIR region for in vivo studies, the development of targeted QDs is essential to achieve specific and reliable in vivo imaging at the target regions.[31−36]

Here, NIR emitting silica-coated PbS QDs were successfully conjugated with a purpose-designed cyclic Arg−Gly−Asp (cRGD) peptide, to obtain a single luminescent and targeted nano-object able to ingeniously merge the selectivity of the peptide toward integrin $\alpha v\beta 3$, and the photostability and peculiar luminescence properties of the inorganic QDs. The $\alpha v\beta 3$ integrin receptor has emerged as an appealing target for diagnostic imaging, because it is overexpressed on some tumor cells and on activated and rapid growing endothelial cells when tumor angiogenesis occurs, whereas it remains not easily appreciable in normal endothelial cells and organs.[37−39] Therefore, a variety of peptide probes, based on the linear and cyclic RGD peptides, that are able to strongly bind with the $\alpha v\beta 3$ receptor were developed to target angiogenic vessels.[22,40−43]

In this work, these emitting single object nanostructures were thoroughly investigated, assessing how the NIR emitting properties are retained upon QD encapsulation into the silica shell, and elucidating the morphology, size, colloidal stability, and surface charge of the resulting silica-coated PbS QDs, before and after their conjugation with cRGD peptide, by means of complementary techniques, such as transmission electron microscopy (TEM), dynamic light scattering (DLS), and ζ-potential measurements.

In vitro studies were performed on human melanoma cells (WM266), which overexpress $\alpha v\beta 3$ integrin.[44] Confocal microscopy investigation confirmed the cell internalization of the silica-coated PbS QDs conjugated with the cRGD peptide, and finally, cytometric analysis established their selectivity for the $\alpha v\beta 3$ integrin receptor. The proposed cRGD peptide PbS QD silica-coated system, thanks to its high colloidal stability in physiological media and the ability to preserve the relevant optical properties in the NIR region, holds great promise as an optical integrin-targeted nanoprobe for in vivo NIR molecular imaging applications.

2. MATERIALS AND METHODS

2.1. Materials. Lead(II) oxide (PbO, powder 99.99%), hexamethyldisilathiane (HMDS, synthesis grade), 1-octadecene (ODE, 90% technical grade), oleic acid (OLEA, technical grade 90%), trioctylphosphine (TOP, 90% technical grade), aqueous ammonia (NH_4OH, 28−30% H_2O), tetraethyl orthosilicate (TEOS, 98%), poly(oxyethylene) (5) nonylphenylether branched (Igepal CO-520), 3-aminopropyltriethoxysilane (APS, 97%), bis(sulfosuccinimidyl)-suberate (≥95%, BS3), paraformaldehyde, Triton X-100, IR125 Dye (dye content 80%), 3-(4,5-dimethylthiazolyl-2)-2,5-diphenyltetrazolium bromide (MTT), tetramethylrhodamine B isothiocyanate functionalized phalloidin (Phalloidin-TRITC), fluoroshield with 4′,6-diamidino-2-phenylindole (DAPI), and ninhydrin were acquired from Sigma-Aldrich. 2,6-Lutidine (98%) was purchased from Alfa Aesar. Phosphate-buffered saline (PBS), tris(hydroxymethyl) aminomethane hydrochloride (Tris−HCl), and borate buffers were prepared by using reagent-grade salts purchased from Sigma. Polypropylene reaction and sintered polyethylene frits were purchased from Alltech Italia (Milan, Italy). Dichloromethane (DCM), acetonitrile (ACN), and diethyl ether were acquired from VWR International (Milan, Italy). Cyanohydroxyimino-acetic acid ethyl ester (Oxyma), 2-(1*H*-benzotriazole-1-yl)-1,1,3,3-tetramethyluronium hexafluorophosphate (HBTU), NovaSyn TGR resin, and all amino acids were acquired from Novabiochem-Merck (Nottingham, U.K.). Piperidine, Kaiser test, *N*,*N*′-diisopropylethylamine (DIPEA), fluorescein isothiocyanate (FITC), trifluoroacetic acid (TFA), scavengers, *N*,*N*-dimethylformamide (DMF), and *N*-methylmorpholine (NMM) were provided by Carlo Erba Reagents (Milan, Italy).

Fetal bovine serum (FBS), Dulbecco's modified Eagle's medium (DMEM), streptomycin (100 μg/mL), and penicillin (100 U/mL) were provided by EuroClone. Petri dishes and disposable culture flasks were purchased from Corning (Glassworks). Water obtained from a Milli-Q gradient A-10 system (Millipore, 18.2 MΩ cm, organic carbon content ≥4 μg/L) was used to prepare all aqueous solutions. All solvents (Sigma-Aldrich) were of the highest purity obtainable.

2.2. Peptide Synthesis. The synthesis of RGD-Nano-FITC and GK-Nano-FITC peptides was manually performed by exploiting the Fmoc solid-phase strategy (0.1 mmol) and by using the NovaSyn TGR resin (loading 0.25 mmol/g) and all standard amino acids. The preactivation of the amino acids (5-fold excess) was achieved by treatment, for 5 min, with HBTU (4.8 equiv)/Oxyma (4.8 equiv)/DIPEA (10 equiv) in DMF, and subsequently they were introduced in the resin suspension in DMF. After 1 h, the reaction was stopped and the Kaiser test was carried out to evaluate the coupling efficiency. The removal of the Fmoc protecting group was performed by using 30% piperidine in DMF (3 × 10 min). For GK-Nano peptide, after the coupling of the Ala residue, Fmoc-βAla-OH was inserted to perform the following labeling with FITC.

In the case of RGD-Nano peptide, the allyl group from Glu5 residue was removed by treatment of the peptidyl resin with $PhSiH_3$ (24 equiv)/$Pd(PPh_3)_4$ (0.25 equiv) in DCM (3 × 10 min), and then the final Fmoc deprotection of Lys1 was achieved. The resin with PyBop (1.5 equiv)/HOBT (1.5 equiv)/DIPEA (2 equiv) in DMF was employed to promote the cyclization reaction between αNH of Lys1 and αCO of Glu5 for 3 h, and the Kaiser test was performed to monitor it. Once the synthesis of RGD-Nano was completed, a treatment of the peptidyl resin with a solution of 2% hydrazine in DMF (20 × 3 min) was performed. FITC labeling was carried out, for

DOI: 10.1021/acsami.7b14155
ACS Appl. Mater. Interfaces 2017, 9, 43113−43126

both peptides, with FITC (2 equiv) and NMM (4 equiv) in DMF for 5 h, to remove the ivDde protecting group from the ε-amino group of the lysine. The peptides were treated with a mixture of TFA/water/triisopropylsilane (95:2.5:2.5 v/v/v) for 3 h at room temperature to cleave off the resin. After the filtration of the resins, the precipitation of the crude peptides was induced by diethyl ether. Subsequently, they were solubilized in H_2O/ACN solution and finally lyophilized. The purification of the products was achieved by preparative reversed-phase high-performance liquid chromatography (RP-HPLC). Namely, a Shimadzu system equipped with a UV−visible detector SPD10A and a Phenomenex Jupiter Proteo column (21.2 × 250 mm^2; 4 μm; 90 Å) was used, and a linear gradient of H_2O (0.1% TFA)/ACN (0.1% TFA) from 5 to 70% was realized in 30 min at a flow rate of 20 mL/min. Lyophilization of the peptides recovered as collected fractions was performed. An AGILENT Q-TOF liquid chromatography/mass spectrometry (LC/MS) instrument equipped with a diode array detector combined with a dual electrospray ionization source on a Phenomenex Aeris Peptide C18 column (2.1 × 50 mm^2; 3.6 μm) was used to assess the identity and purity of the compounds. A flow rate of 200 μL/min and a linear gradient of H_2O (0.01% TFA)/ACN (0.01% TFA) from 5 to 70% of ACN in 15 min was exploited.

2.3. Synthesis of PbS Quantum Dots. The synthesis of PbS QDs was carried out by introducing 4 mmol of PbO, 9.0 mL of trioctylphosphine (TOP), and 2 g of oleic acid (OLEA) in a three-neck flask, previously filled with 36 mL of 1-octadecene (ODE).[45] The formation of lead-oleate precursors was promoted by stirring the reaction mixture under vacuum at 110 °C upon quick injection of a solution containing the sulfur precursor (20 mM) and hexamethyldisilathiane (HMDS) in ODE, thus achieving a Pb/S molar ratio of 2:1. The inhibition of further nucleation as well as promotion of the growth of the freshly formed nuclei were achieved by sudden cooling to 80 °C immediately after the injection. The reaction was finally stopped at given times, depending on the QD final size. Namely, QDs having a size of about 2.4, 2.6, and 3.0 nm were obtained at a growth time of 8, 10, and 13 min, respectively. Each sample of PbS QDs was purified and recovered by addition of ethanol and subsequent precipitation by centrifugation (three cycles). Finally, the QDs were dispersed in organic solvent.

2.4. Preparation of Silica-Coated PbS Quantum Dots. A water-in-oil (W/O) microemulsion approach[26] was exploited to grow the silica shell on the PbS QD surface.[28,29,46−48] The influence of PbS QD, ammonia, and TEOS concentration on the morphology of the final shell was investigated. The tested concentrations of PbS QDs were 2.5 × 10^{-5}, 2.0 × 10^{-5}, 1.3 × 10^{-5}, and 9.0 × 10^{-6} M, and the investigated volumes of TEOS solution were 20, 30, 40, and 50 μL. Igepal CO-520 (350 μL), ammonia solution (200 μL), and TEOS were introduced into 6 mL of cyclohexane PbS QD solution to form the inverse microemulsion at 28 °C. After 20 h, methanol (∼10 mL) was added to the reaction mixture and finally the silica-coated PbS QDs (PbS QD@SiO_2 NPs) were then recovered by centrifugation, washed, and dispersed in ethanol.

2.5. Grafting of PbS@SiO_2 Nanoparticle Surface with Primary Amine Groups. The formation of hydrogen bonds between hydroxyl groups on PbS QD@SiO_2 NPs and APS molecules was promoted by mixing 9 mL of a PbS QD@SiO_2 NP solution (2.8 × 10^{13} part/mL or 4.5 × 10^{-11} mol/mL) with 1 mL of a APS solution in ethanol (0.29 M), for 2 h, at room temperature.[26] Subsequently, the reaction mixture was kept at 80 °C for 1 h, thus allowing the creation of covalent bonds and release of water molecules. Finally, the PbS QD@SiO_2 NPs decorated by amine groups were purified and dispersed in 1.5 mL of a borate buffer (50 mM, pH 8.5)/DMSO mixture (1:1).

The evaluation of the amount of primary amine groups introduced in the PbS QD@SiO_2 NP solution was performed via ninhydrin assay.[29] APS standard solutions (5 μM−15 mM) were treated with an excess of the ninhydrin solution (3 × 10^{-5} M) at 90 °C for 5 min. A calibration curve was obtained by plotting the solution absorption intensity at 570 nm versus APS concentration, thus calculating the extinction coefficient, which approached 950 [L/(mol cm)]. The ninhydrin test was then performed on the prepared PbS QD@SiO_2 NPs to calculate the concentration of amine groups available in the sample (nearly 0.3 mM), finally corresponding to 2000 amine groups per NP (considering the sample formed of nearly 10^{14} NPs).

2.6. Two-Step Bioconjugation of Amine-Functionalized PbS@SiO_2 Nanoparticles with GK-Nano-FITC or RGD-Nano-FITC Peptide. First, 1.0 mL of amine-functionalized PbS QD@SiO_2 NP (NH_2-PbS QD@SiO_2 NPs) dispersion (C_{NPs} = 2 × 10^{-7} M and C_{NH_2} =1.5 × 10^{-3} M) was added to 0.5 mL of BS3 solution (5 × 10^{-2} M). The amide forming reaction between silica-coated NPs and BS3 was carried out in a borate buffer (50 mM, pH 8.5)/DMSO mixture (1:1) for 30 min at 20 °C under mild stirring. The BS3-activated NH_2-PbS QD@SiO_2 NPs were then recovered by centrifugation at 7000*g* for 20 min to remove the excess BS3 molecules. The final particle pellet was dispersed in 1.5 mL of borate buffer (50 mM, pH 8.5)/DMSO mixture (1:1) containing GK-Nano-FITC or RGD-Nano-FITC peptide (2.5 × 10^{-4} M) and left to react for 2 h at 20 °C under mild stirring. The reaction was quenched by addition of Tris−HCl buffer at a final concentration of 30 mM (pH 7.5) for 15 min at 20 °C. Finally, the peptide-conjugated NPs were centrifuged (7000*g*) and washed three times with PBS. The NPs were dispersed in PBS, sonicated, and stored at 4 °C until use.

The amount of peptide covalently linked to the surface of the peptide/PbS QD@SiO_2 NP conjugates was determined by photoluminescence (PL) measurements, according to a previously reported experimental procedure.[22] The area underlying the curve of the PL emission band was measured in the wavelength range between 500 and 650 nm.

2.7. Cell Culture. DMEM and Roswell Park Memorial Institute (RPMI) 1640 nutrient, supplemented with heat inactivated FBS (10%), L-glutamine (2 mM), penicillin (100 U/mL), and streptomycin (100 μg/mL) were used for the culture of human melanoma WM266 cell lines.[22]

2.8. Cytotoxicity Assays. Cytotoxicity of GK-Nano-FITC peptide/PbS QD@SiO_2 NP and RGD-Nano-FITC peptide/PbS QD@SiO_2 NP conjugates was assessed by MTT assay and expressed as IC_{50} values.[49] Cells were dispensed into 96-well plates at a density of 5000 cells/well and incubated for 24 h at 37 °C with 5% CO_2. Peptide/PbS QD@SiO_2 NP conjugates in PBS buffer at NP concentrations ranging from 340 to 0.5 nM (5.1−0.0108 μM in terms of GK-Nano-FITC or RGD-Nano-FITC peptide) were added to each well starting with PBS stock solutions of 500 nM NP, 7.5 μM RGD-Nano-FITC, and 10.8 μM GK-Nano-FITC peptide. Subsequently, the MTT assay was performed according to the previously reported procedure[22,49] and by using a PerkinElmer 2030 multilabel reader Victor TM X3. The control was represented by untreated cells.

2.9. Cytofluorimetric Analysis of Peptide/PbS QD@SiO_2 NP Conjugates. WM266 cells were seeded in 60 mm dishes at a density of 500 000/well and subsequently incubated for 30 or 120 min at 37 °C with GK-Nano-FITC peptide/PbS QD@SiO_2 NP or RGD-Nano-FITC peptide/PbS QD@SiO_2 NP conjugates at the same concentration in terms of FITC (100 nM). After incubation, cells were washed twice with cold PBS buffer solution, detached with trypsin-ethylenediaminetetraacetic acid, and washed again with cold PBS buffer solution, then the pellet was resuspended with PBS (300 μL). Control samples were represented by untreated cells. In particular, the cellular uptake of both types of conjugates was quantitatively evaluated by analyzing the cell samples using the BD LSRFortessa X-20 (Becton, Dickinson, and Company, Franklin Lakes, NJ) cell analyzer. For each measurement, 10 000 data samples were collected using a flow rate of 12 μL/min. The samples were excited with a 488 nm laser (laser power 50 mW), and the emission was detected through a 525(±25) nm bandpass filter.

2.10. Absorption and Emission Spectroscopic Investigation of Nanoparticles. Vis−NIR absorption spectra were recorded by using a Cary Varian 5000 UV−visible−NIR spectrophotometer and optically coupled quartz cuvettes (optical length = 1 mm). A Horiba Jobin Yvon Fluorolog-3 spectrofluorimeter, equipped with a 450 Xe lamp as excitation source, coupled to a double grating Czerny−Turner monochromator was used for the PL emission measurements.[26] IR125 dye in ethanol was employed as a standard to determine the relative

DOI: 10.1021/acsami.7b14155
ACS Appl. Mater. Interfaces 2017, 9, 43113−43126

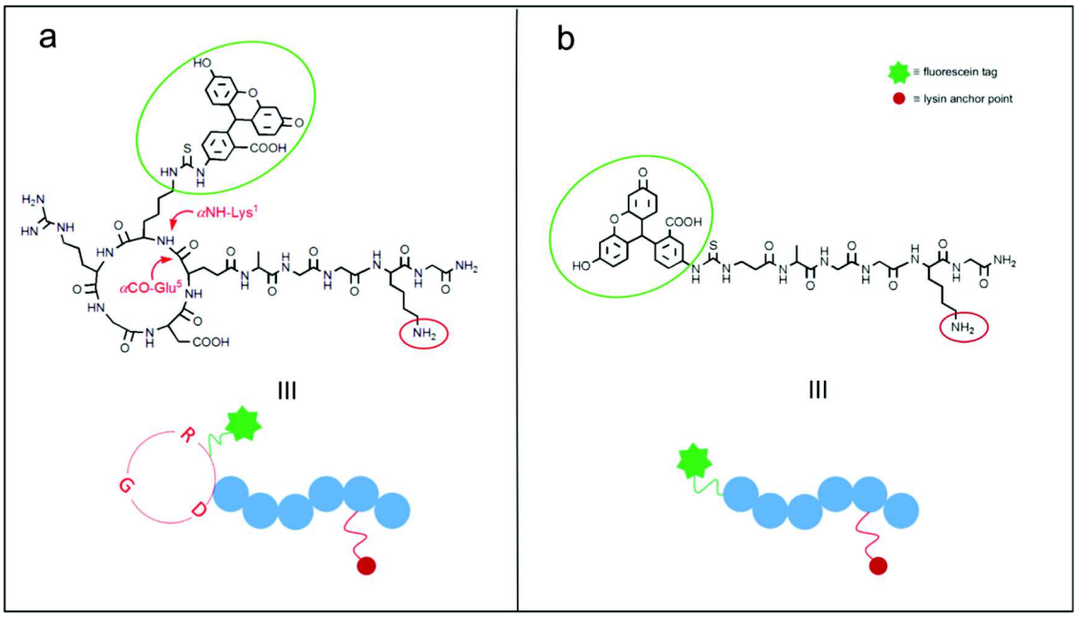

Figure 1. Chemical structure and corresponding sketch of (a) RGD-Nano-FITC and (b) GK-Nano-FITC peptides.

PL quantum yield (QY), excited at 650 nm, and QY was calculated using the equation reported in the Electronic Supporting Information (eq S1, see Supporting Information).

2.11. Attenuated Total Reflection-Fourier Transform Infrared (ATR-FTIR) Spectroscopic Investigation. A PerkinElmer Spectrum One Fourier transform infrared (FTIR) spectrometer equipped with a deuterated triglycine sulfate (DTGS) detector was used to record the infrared spectra with 4 cm^{-1} spectral resolution. The attenuated total reflection (ATR) measurements were carried out by using a diamond microprism (three bounce, diameter 4 mm) as the internal reflection element (IRE). The measurements were performed by casting the samples (10 μL) directly on the upper face of the diamond crystal after complete evaporation of the solvent.

2.12. Morphological Characterization of Nanoparticles. Transmission electron microscopy investigation of the NPs was accomplished by means of a Jeol Jem-1011 microscope (accelerating voltage of 100 kV, Quemesa Olympus CCD 11 Mp Camera). A PbS QD cyclohexane dispersion, or alternatively a PbS@SiO_2 NP ethanol dispersion, was deposited on a 300 mesh amorphous carbon-coated Cu grid by dipping. Freeware ImageJ analysis program was used to determine the size statistical analysis, expressed as NP average size and size distribution (as relative standard deviation, $\sigma_{\%}$) of the samples. For field-emission scanning electron microscopy (FE-SEM), measurements were performed by means of a Zeiss Sigma microscope (working voltage of 0.5−20 kV, in-lens secondary electron detector) on sample deposited on double-sided carbon tape glued on stainless-steel sample holders.

2.13. Investigation of Particle Size, Size Distribution, and Colloidal Stability. Hydrodynamic diameter and surface charge of the PbS@SiO_2 NPs were determined by means of a Zetasizer Nano ZS, Malvern Instruments Ltd., Worcestershire, U.K. (DTS 5.00). In particular, size and size distribution (in terms of polydispersity index (PDI)) of functionalized silica-coated NPs, dispersed in borate buffer (50 mM) at pH 8.5 and diluted with filtered water (0.22 μm, Advantec MFS, Pleasanton, CA), were obtained by dynamic light scattering (DLS) analysis. The ζ-potential measurements were performed by diluting functionalized silica-coated NPs dispersed in borate buffer (50 mM, at pH 8.5) with prefiltered (CA, 0.22 μm) KCl aqueous solution (1 mM) and by using a laser Doppler velocimetry. All presented data were calculated as mean values ± standard deviation of three replicates.

2.14. Confocal Microscopy Investigation. The in vitro investigation, by means of laser scanning confocal microscopy, of the cellular uptake of RGD-Nano-FITC peptide/PbS QD@SiO_2 NP conjugates was achieved by using a Leica TCS SP8 X (Leica Microsystems, Germany) upright confocal microscope using a 63×, 1.40 numerical aperture oil immersion lens for imaging. DAPI, visible fluorescently labeled RGD-Nano-FITC peptide/PbS QD@SiO_2 NP conjugates, and Phalloidin-TRITC were detected by setting the laser beams at excitation wavelengths of 405, 488, and 568 nm, respectively. The use of sequential scanning allowed possible cross-talk to be eliminated. Furthermore, an increase of the signal-to-noise response was achieved by using a four line average. The Leica LAS AF LITE software (Leica microsystems, Germany) was used to process the overall data. WM266 cells (2×10^4 cells/well) were grown on Lab-Tek Chamber Slides (8 wells) for 24 h and then exposed for 30 or 120 min to RPMI containing RGD-Nano-FITC peptide/PbS QD@SiO_2 NP conjugates. The tested NP concentration was 20 nM (400 nM in terms of FITC). After treatment with NPs and removal of the culture medium, cells were rinsed three times with PBS buffer and then fixed by exposing to 4% w/v paraformaldehyde in PBS buffer for 15 min. After washing with PBS buffer (twice), permealization of cells with Triton X-100 0.1% in PBS for 10 min was performed, and subsequently they were washed again with the same buffer. A blocking phase on the cells with BSA (bovine serum albumin, 5% (w/v) in PBS) was followed by incubation at 37 °C with TRITC-conjugated Phalloidin (1 μM) for 60 min as F-actin marker. After staining, cells were washed twice with Milli-Q water, a drop of DAPI containing Fluoroshield was added, and they were covered with a glass slide.

3. RESULTS AND DISCUSSION

In this work, a suitably designed peptide, containing a cRGD motif for targeted molecular bioimaging, was covalently conjugated to the surface of luminescent silica NPs with emitting properties in the NIR region. Firstly, a silica shell was grown on the surface of the hydrophobic PbS QDs to achieve good stability in aqueous media.

Indeed, silica is a material characterized by good biocompatibility, optical transparency, and chemical inertness; furthermore, it is able to lower the release of toxic metal ions, retain the QD optical properties, and limit photoinduced degradation processes occurring at their surface. The silanization process was carried out by properly adjusting the size, shape, and surface charge of the silica-coated PbS QDs to promote their

DOI: 10.1021/acsami.7b14155
ACS Appl. Mater. Interfaces 2017, 9, 43113−43126

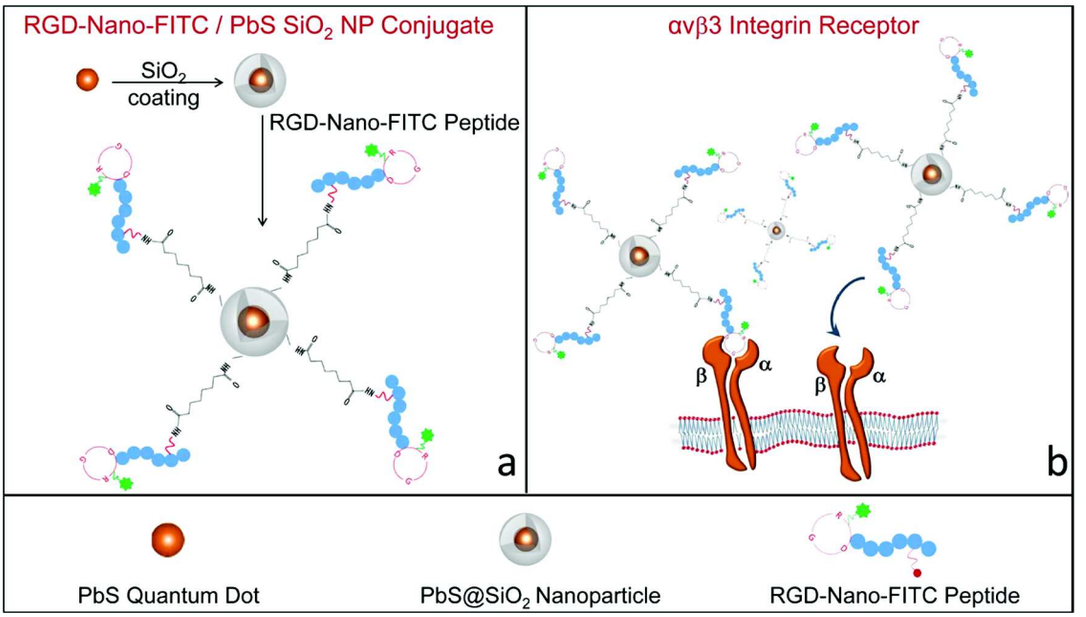

Figure 2. Schematic illustration of (a) PbS QD@SiO_2 NP functionalization by growth of silica shell and their binding to the RGD-Nano-FITC peptide to achieve the subsequent (b) molecular recognition between RGD-Nano-FITC/PbS QD@SiO_2 NP conjugates and the $\alpha v\beta 3$ integrin receptors.

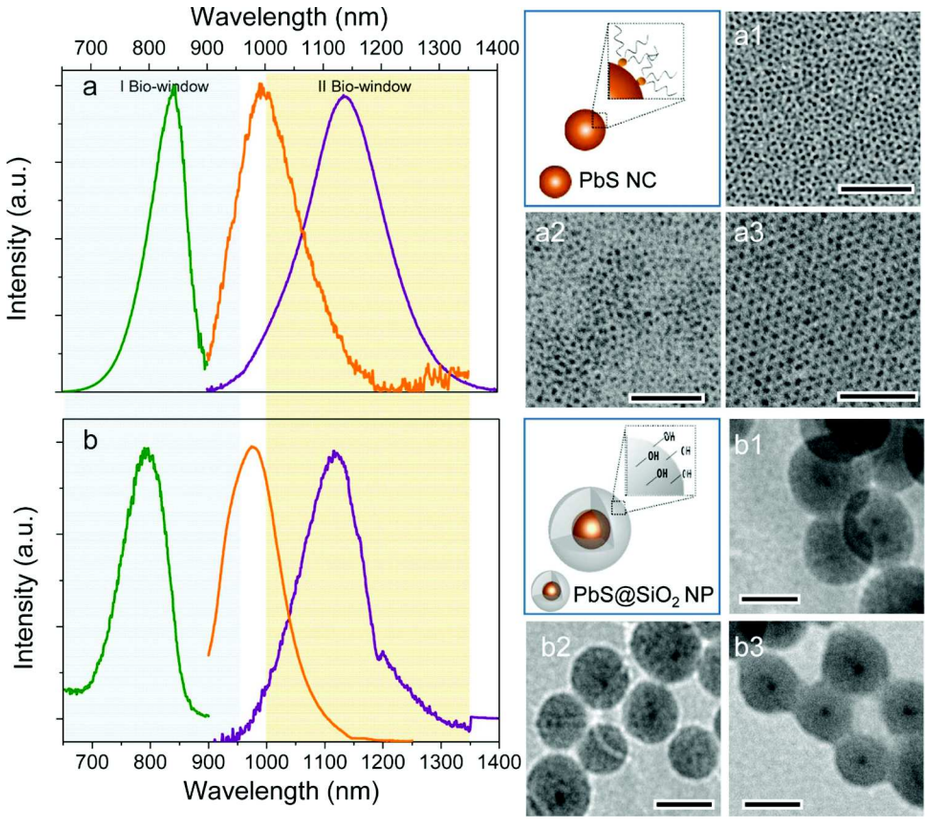

Figure 3. PL emission spectra and TEM micrographs (scale bar = 50 nm) of OLEA/TOP capped PbS QDs dispersed in toluene with average diameters of 2.4 nm (a, green line, a1), 2.6 nm (a, orange line, a2), and 3.0 nm (a, violet line, a3). PL emission spectra and TEM micrographs (scale bar = 25 nm) of silica-coated PbS QDs dispersed in ethanol obtained starting from OLEA/TOP capped PbS QDs with average diameters of 2.4 nm (b, green line, b1), 2.6 nm (b, orange line, b2), and 3.0 nm (b, violet line, b3). All PL emission spectra were recorded using a λ_{exc} of 650 nm.

dispersibility in physiological solution and ultimately control the characteristics involved in the cell internalization pathways,

DOI: 10.1021/acsami.7b14155
ACS Appl. Mater. Interfaces 2017, 9, 43113−43126

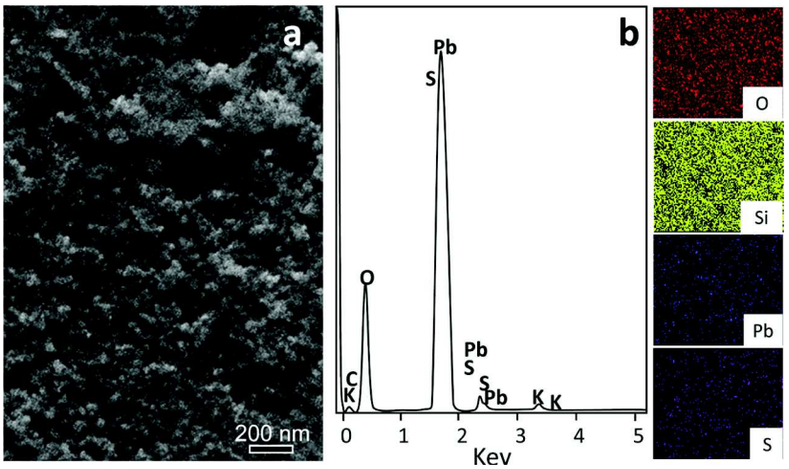

Figure 4. SEM−EDX analysis: SEM micrograph of silica-coated PbS QDs (20 kV) (a), EDX elemental spectrum (b) and EDX maps of oxygen (red), silicon (yellow), lead (blue), and sulfur (purple) in the sample.

still preserving their colloidal stability and optical properties. Amine-functionalized silica-coated PbS QDs were then conjugated with $\alpha v\beta 3$ integrin-targeting ligand molecules.

In particular, the bioconjugation process was carried out by exploiting, alternatively, two different peptides with fluorescent properties in the visible light region, namely, RGD-Nano-FITC and GK-Nano-FITC (Figure 1) peptides. The RGD-Nano-FITC peptide is a bifunctional molecule consisting of both a linear and a cyclic portion. The former presents an amine group (from lysine residue of the GK motif) as an anchor point for the surface of the amine-functionalized silica-coated PbS QDs.[50−55] The latter portion contains the RGD epitope for integrin-specific binding and a lysine residue for functionalization with FITC (Figure 1). Such a dye, emitting in the visible region, was purposely introduced into the peptide structure to quantitatively evaluate the actual amount of peptide covalently linked to the amine-functionalized silica-coated PbS QDs, and, importantly, to ensure feasibility in the visible range of confocal microscopy and flow cytometry studies of the cellular uptake process.

The GK-Nano-FITC peptide, containing only the linear portion, was used as a control system to achieve GK-Nano-FITC/PbS QD@SiO_2 NP conjugates to be evaluated against the RGD-Nano-FITC/PbS QD@SiO_2 NP conjugates for investigating the capability of the RGD sequence to accomplish the selective targeting.

Figure 2 shows a schematic illustrating the main steps starting from the growth of the silica shell on the PbS QDs for preparation of the RGD-Nano-FITC conjugates.

3.1. Silica-Coated PbS Quantum Dots. The synthetic parameters were properly controlled to tune the size of the PbS QDs, which, accordingly, resulted in size-dependent emission in the first and second NIR window of the electromagnetic spectrum. For this purpose, thermal decomposition of suitable organometallic precursors in coordinating solvents was promoted to synthesize different QDs with three different sizes. The QD size was controlled by varying the reaction times. TEM investigation proved the formation of samples of PbS QDs with uniform size having three different average diameters, equal to 2.4 ± 0.5 nm (Figure 3a1), 2.6 ± 0.5 nm (Figure 3a2), and 3.0 ± 0.5 nm (Figure 3a3). The corresponding emission band, progressively red shifting with increasing core size, clearly shows a single narrow emission peak, due to a band-edge recombination, centered at 845 (Figure 3a, green line), 991 (Figure 3a, orange line), and 1135 nm (Figure 3a, violet line) for PbS QDs of 2.4, 2.6, and 3.0 nm, respectively.

QDs were embedded in a silica shell by exploiting a water-in-oil microemulsion method,[26,28,29,46−48] thus resulting in core−shell nanostructures (PbS@SiO_2 NPs) characterized by PL emission properties in the NIR region. Starting from PbS QDs of 2.4, 2.6, or 3.0 nm, respectively, silica shells were grown at the QD surface at a fixed volume of Igepal (350 μL) and ammonia solution (200 μL). In particular, the effect of silica growth parameters, namely, PbS QD concentration and silica precursor molar ratio, on the size, morphology, and optical properties of the resulting silica NPs was monitored by TEM analysis and UV−vis absorption and PL emission spectroscopy (Figures S1 and S2, see Supporting Information).[26] The TEM micrograph clearly demonstrated that core−shell structures, with elevated yield and without formation of empty silica NPs, were synthesized only when using 9×10^{-6} M PbS QD samples and a TEOS concentration of 1.5×10^{-2} M. TEM investigation proved the formation, starting from PbS QD core sizes of 2.4, 2.6, and 3.0 nm, respectively, of spherical PbS QD@SiO_2 NPs, with a very uniform shell and a narrow size distribution, with an average diameter of 29(±3) nm ($\sigma_{\%}$ = 10%, Figure 3b1), 30(±4) nm ($\sigma_{\%}$ = 13%, Figure 3b2), and 27(±4) nm ($\sigma_{\%}$ = 15%, Figure 3b3), corresponding to a silica shell thickness of about 13, 14, and 12 nm, respectively. In all cases, the preparation of single PbS QD core silica NPs was achieved without empty silica NPs.

The PL spectroscopic investigation performed on the three silica-based PbS QD nanostructure samples (PbS QD@SiO_2 NPs) demonstrated that the PbS QD emission was preserved after their incorporation into the silica shell (Figure 3b). Namely, a PL peak was detected at 790, 974, and 1115 nm for the PbS QD@SiO_2 NPs with a QD core of 2.4, 2.6, and 3.0 nm, respectively, thus indicating, in all investigated cases, a slight blue shift from the position of the "as prepared" PbS QD emission in toluene solution (Figure 3a,b). As previously reported, the PL peak blue shift can be reasonably ascribed to the removal of the capping agents from the as prepared PbS QDs and their replacement with TEOS molecules. These phenomena are expected to result in the formation of a very thin layer of oxide on the surface that ultimately induces a reduction of the size of the pristine PbS QD core.[26]

DOI: 10.1021/acsami.7b14155
ACS Appl. Mater. Interfaces 2017, 9, 43113−43126

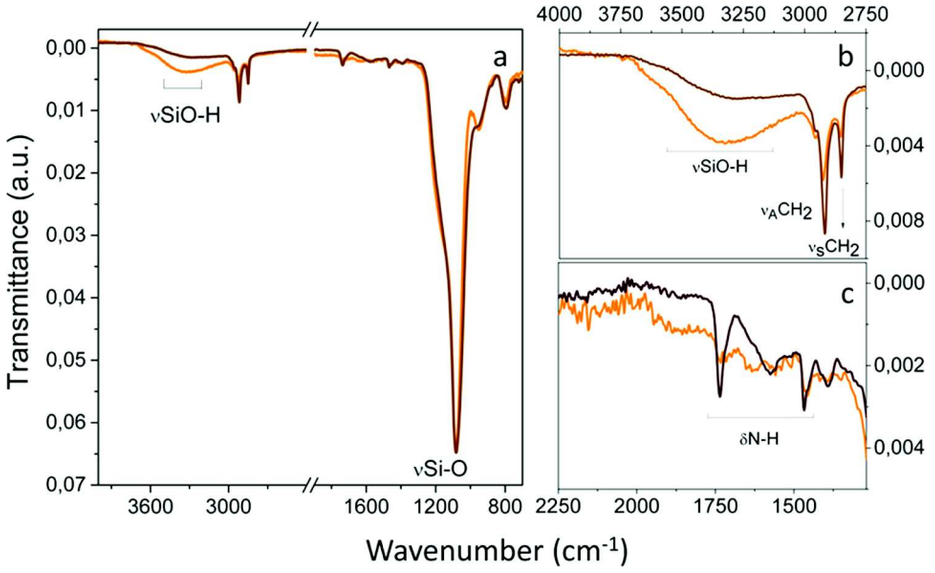

Figure 5. ATR-FTIR spectrum of PbS QD@SiO_2 NPs (red wine line, a) and amine-functionalized PbS QD@SiO_2 NPs (orange line, a). Detail of ATR-FTIR spectrum in the regions between 4000−2750 cm^{-1} (b) and 2250−1250 cm^{-1} (c).

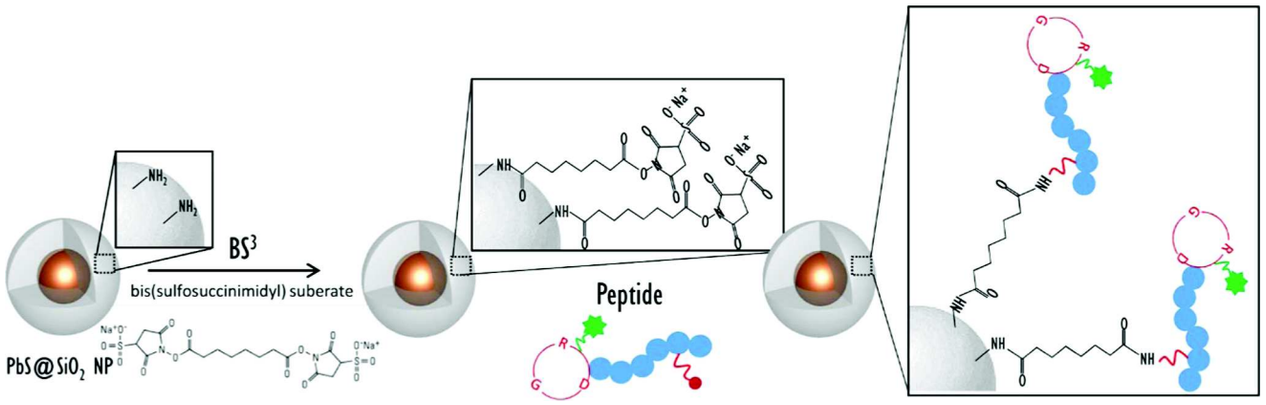

Figure 6. Schematic representation of the conjugation reaction of PbS QD@SiO_2 NPs with RGD-Nano-FITC peptide by cross-coupling reaction mediated by BS3.

Scanning electron microscopy (SEM) investigation was performed on the PbS QD@SiO_2 NPs obtained from PbS QDs of 2.6 nm (Figure 4a), confirming the formation of spherical and very uniformly shaped silica-based beads, in agreement with TEM observations. The SEM−energy-dispersive X-ray (EDX) elemental spectrum recorded on a typical PbS QD@SiO_2 NP sample is reported in Figure 4b, showing the characteristic peaks of lead and sulfur, as well as those of silicon and oxygen. EDX mapping images of these elements are also shown in Figure 4b. The investigation carried out on the other samples provided comparable results.

3.2. Bioconjugation of the PbS QD@SiO_2 Nanoparticles with the cRGD Motif-Containing Peptides. Prior to conjugation with the peptides, primary amine groups were grafted onto the PbS silica NP surface by reaction with APS, thus representing efficient anchor points for the subsequent covalent binding with the NH_2 groups present in the peptide structures.

The functionalization of the NP silica shell with amine groups was demonstrated by means of a reaction with ninhydrin, carried out according to a previously reported experimental procedure (see Materials and Methods section).[26,29,47]

The ATR-FTIR spectrum of the PbS QD@SiO_2 NPs with PbS QD cores of 2.6 nm after functionalization with APS was compared to that recorded for the as prepared NPs (Figure 5). The intensity of the particular band ascribed to the stretching of SiO−H groups clearly decreases in the PbS QD@SiO_2 NP spectrum (Figure 5b, red wine line) when compared to that of the as prepared NPs (Figure 5b, orange line), which is due to the binding of the NH_2 groups on the silica surface as a result of the reaction with APS molecules. The grafting of the NH_2 groups at the NP surface was also demonstrated by the occurrence of the two signals centered at 1580 and 1650 cm^{-1}, ascribed to the bending of N−H, clearly visible in the spectra of the functionalized PbS QD@SiO_2 NPs (Figure 5c). Similar results were obtained performing the ATR-FTIR characterization on silica-coated NPs having a PbS QD core of 2.4 and 3.0 nm (data not shown).

The bioconjugation process was carried out starting from PbS QD@SiO_2 NPs with a core of 2.6 nm, however, it can be safely extended to the silica-coated NP samples with a PbS QD

DOI: 10.1021/acsami.7b14155
ACS Appl. Mater. Interfaces 2017, 9, 43113−43126

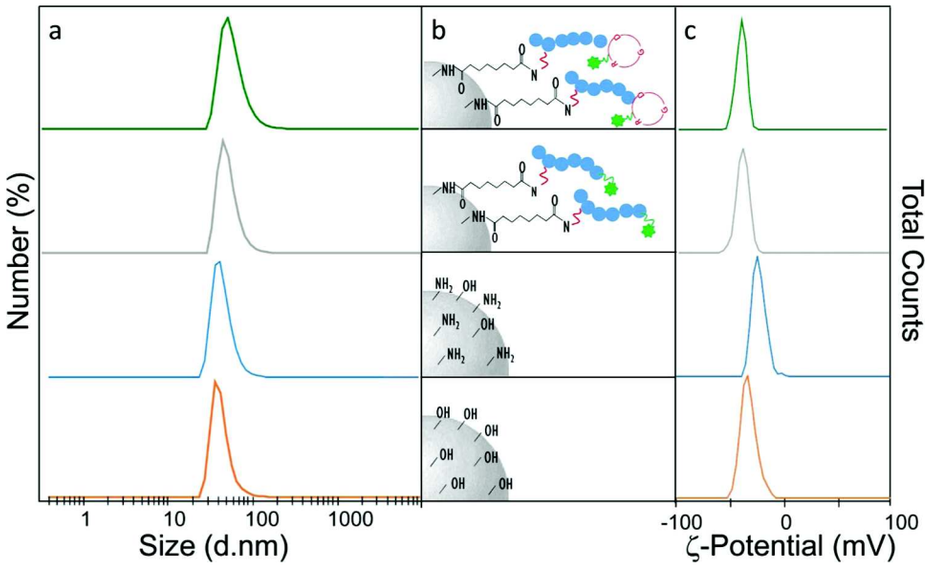

Figure 7. Size distribution recorded by DLS (a) and ζ-potential measurements (c) of PbS@SiO_2 NPs (red line), amine grafted PbS@SiO_2 NPs (blue line), GK-Nano-FITC/PbS SiO_2 NP conjugates (gray line), and RGD-Nano-FITC/PbS SiO_2 NP conjugates (green line). Samples were dispersed in borate buffer (50 mM) at pH 8.5. (b) Sketch of the silica surface at each functionalization step.

core of 2.4 and 3.0 nm, considering the identical surface chemistry of the structures. The reaction is based on the achievement of covalent conjugation between the NH_2 groups at the PbS QD@SiO_2 NP surface and those present in each peptide. Namely, GK-Nano-FITC or RGD-Nano-FITC peptides were bound to the PbS QD@SiO_2 surface by means of a crosslinker, BS3, as shown in Figure 6. The concentration of the two different peptides conjugated to the PbS SiO_2 NP surface was estimated, by PL measurements, to be 10.8(±0.4) × 10^{-6} M and 7.5(±0.3) × 10^{-6} M for the GK-Nano-FITC and RGD-Nano-FITC peptides, respectively. The concentration value achieved for RGD-Nano-FITC peptide was found to be slightly lower than that obtained for the GK-Nano-FITC peptide, thus indicating a decrease of the coupling reaction yield, which can be reasonably explained considering the larger size of the RGD-Nano-FITC peptide molecules, which may hamper their effective binding to the surface of the PbS silica NP surface, thus limiting the conjugation yield, as also reported previously.[22]

A structural investigation of the two luminescent nanostructured conjugates was carried out by means of DLS and ζ-potential analysis, as size and surface charge are essential parameters regulating the cellular internalization pathway and the consequent NP intracellular fate.

Hydrodynamic diameter and surface charge density of the PbS@SiO_2 NPs were recorded for the as synthesized PbS@SiO_2 NPs, the amine-functionalized PbS@SiO_2 NPs, and finally for GK-Nano-FITC and RGD-Nano-FITC, respectively, conjugated to the PbS@SiO_2 NPs (Figure 7).

DLS analysis clearly indicated, throughout the procedure, the occurrence of a monomodal size distribution, thus ruling out any significant aggregation of silica-based nanostructures in the aqueous medium. Namely, average diameters of 48 (PDI 0.161 ± 0.014), 50 (PDI 0.179 ± 0.018), 65 (PDI 0.235 ± 0.021), and 68 nm (PDI 0.219 ± 0.018) were recorded for as synthesized PbS QD@SiO_2 NPs, amine-functionalized PbS QD@SiO_2 NPs, GK-Nano-FITC/PbS QD@SiO_2 NP conjugates, and RGD-Nano-FITC/QD PbS SiO_2 NP conjugates, respectively (Figure 7a). No significant change in hydrodynamic diameter was observed when comparing the PbS QD@SiO_2 NPs with the amine-functionalized PbS@SiO_2 NPs, however, an increase of the nanostructure size was recorded after silica NP conjugation with GK-Nano-FITC or RGD-Nano-FITC peptide, which is consistent with the effective binding of the peptides to the NP surface.

The apparent discrepancy in size measured for the as synthesized PbS QD@SiO_2 NPs by TEM (30 nm, Figure 3b2) and by DLS is, in fact, consistent with the ability of TEM to detect just the inorganic portion of the NP. Conversely, the higher hydrodynamic diameter values obtained by DLS investigation (48 nm, Figure 7a red line) result from the whole structure, consisting of the inorganic particle surrounded by the capping agent coordinated to the surface, and including the hydration shell and also the excess of counter ions. Moreover, the NPs are expected to shrink due to the drying process needed to perform TEM analysis.[56] For these reasons, the TEM investigation performed on the amine-functionalized PbS QD@SiO_2 NPs and the GK-Nano-FITC/PbS QD@SiO_2 NP and RGD-Nano-FITC/QD PbS SiO_2 NP conjugates (data not shown) produced the same results as those obtained for the as synthesized PbS QD@SiO_2 NPs, as the technique, under the conditions used for the analysis in this work, is not sensitive to the detection of the organic moieties linked to the NP surface.

ζ-potential measurements indicated that, upon grafting the amine groups, the PbS@SiO_2 NPs having a negative charge (−35.4 ± 3.41 mV, Figure 7b orange line) become less negatively charged (−26.6(±1.2) mV, Figure 7b blue line), as previously reported.[29] The subsequent conjugation reaction with each of the two peptides provides an average ζ-potential value of −40.3(±0.5) mV and −42.2(±0.4) mV for GK-Nano-FITC (Figure 7b, gray line) and RGD-Nano-FITC peptide (Figure 7b, green line), respectively.

The more negative values of the PbS QD@SiO_2 NPs functionalized with the peptides, with respect to the plain −NH_2 grafted silica-coated QDs, can be associated to the lower amount of free amino groups at the NP surface. In particular,

DOI: 10.1021/acsami.7b14155
ACS Appl. Mater. Interfaces 2017, 9, 43113−43126

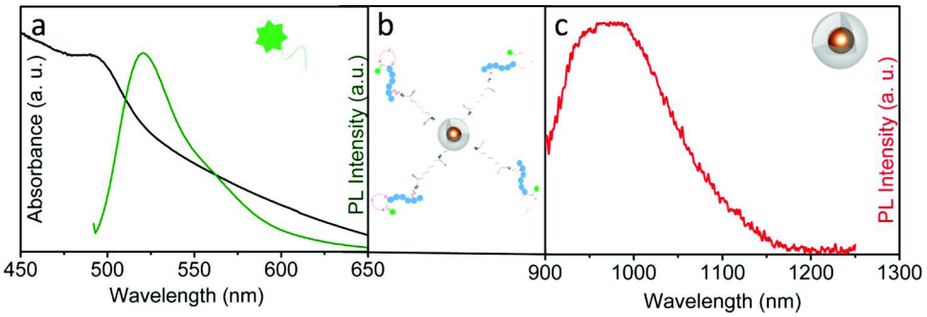

Figure 8. Absorption and PL (λ_{exc} 488 nm) emission spectra of RGD-Nano-FITC/PbS QD@SiO_2 NP conjugates in the visible range (a). PL emission spectrum of RGD-Nano-FITC/PbS QD@SiO_2 NP conjugates in the NIR (λ_{exc} 650 nm) range (c) along with their sketch (b).

the functionalization with either GK-Nano-FITC or RGD-Nano-FITC peptide induces a partial charge neutralization, due to the covalent binding of the amine groups at the surface with the targeting moiety, mediated by the BS3 spacer. Therefore the detected surface charge variation ultimately provides further proof of the effective conjugation reaction.

The success of the bioconjugation was finally demonstrated by the spectroscopic investigation (vis−NIR absorption and PL emission spectroscopy) carried out on the two luminescent nanostructured conjugates. The vis−NIR absorption investigation performed on the RGD-Nano-FITC/PbS QD@SiO_2 NP conjugates results in spectral features that, although resuming the characteristics of the PbS QD@SiO_2 NPs (Figure S3, see Supporting Information), are mainly dominated by the absorption peak centered at 498 nm (Figure 8a, black line) due to the FITC moiety in the RGD-Nano-FITC peptide structure, which is also responsible for the emission peak observed at 530 nm in the visible range (Figure 8a, green line). Interestingly, the emission peak at 974 nm in the RGD-Nano-FITC/PbS QD@SiO_2 NP conjugates (Figure 8c) does not show any shift toward the NIR range (Figure 3b, red line). In addition, the QY efficiency of the PL spectrum was determined for the RGD-Nano-FITC/PbS QD@SiO_2 NP conjugates and compared with those of the as prepared PbS QDs before and after growth of the silica shell (eq S1, see Supporting Information). Namely, the QY efficiency was found to be 18, 14, and 10% for the as synthesized PbS NCs, PbS QD@SiO_2 NPs, and RGD-Nano-FITC/PbS QD@SiO_2 NP conjugates, respectively. The slight QY decrease from 14 to 10%, observed passing from silica-coated PbS NCs to conjugates, can reasonably be ascribed to a pH effect, because alkaline aqueous conditions, exploited for the bioconjugation reaction, can induce the OH^- ions to cross the silica matrix, thus affecting the protonation state of the ligands and therefore their ability to passivate the QD surface.[26] However, the overall data highlighted that the particular optical properties of pristine PbS QDs are retained in the RGD-Nano-FITC/PbS QD@SiO_2 NP conjugates, which thus represent effective probes with great potential for biological imaging.

To exclude any PL contribution due to nonspecific absorption of the RGD-Nano-FITC peptide on the surface of the PbS QD@SiO_2 NPs, incubation of a mixture containing amine-functionalized silica-coated PbS QDs and the free peptide was performed without using any linker, in the same conditions.

After purification, the characteristic emission of the peptide was not detected in the PL spectrum of the purified product, thus allowing the emission to be unequivocally ascribed to the actual conjugation occurring only in the presence of BS3 acting as a crosslinker for the covalent binding between NP and peptide (Figure S4, see Supporting Information).

Further investigation was carried out by means of FTIR-ATR spectroscopy (Figure 9). The spectrum obtained from the

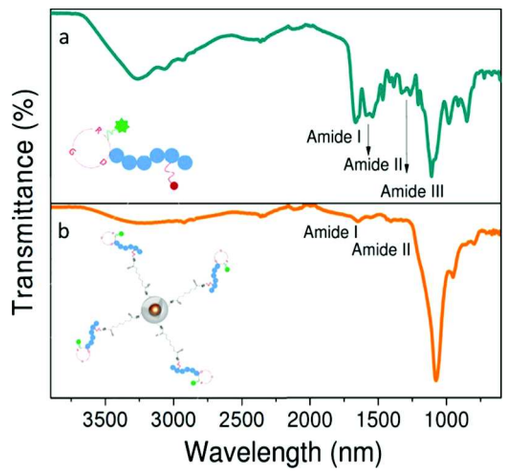

Figure 9. FTIR spectra of the RGD-Nano-FITC peptide (a) and the RGD-Nano-FITC/PbS QD SiO_2 NP conjugates (b).

RGD-Nano-FITC peptide shows C−H and N−H stretching modes in the 3600−2500 cm^{-1} region, and the two maxima at 1660 and 1540 cm^{-1} can be ascribed to the amide I and II bands, respectively. In the 1200−1000 cm^{-1} region, the amide III vibrations and the in-plane aromatic C−H bending vibration can be found. The FTIR-ATR spectrum of the RGD-Nano-FITC/PbS SiO_2 NP conjugates is consistent with the combination of the free RGD-Nano-FITC peptide and the amine-functionalized PbS QD@SiO_2 NP spectra, where the amide I (1660 cm^{-1}) and II (1543 cm^{-1}) modes are still present.[22] Finally, the band centered at 1070 cm^{-1} arises from the combination of the symmetric and asymmetric stretching vibration of Si−O−Si and Si−OH bonds and the amide III vibrations.

Vis−NIR absorption and PL emission optical investigation, as well as FTIR-ATR analysis, performed on GK-Nano-FITC/PbS QD@SiO_2 NP conjugates provided similar results (data not shown).

The overall results of the morphological and spectroscopic characterization confirm the success of the conjugation process and prove the viability of the preparation strategy for effectively achieving NIR and visible emitting nanoprobes with the RGD motif for the targeting of $\alpha v\beta 3$ integrin receptor along with

DOI: 10.1021/acsami.7b14155
ACS Appl. Mater. Interfaces 2017, 9, 43113−43126

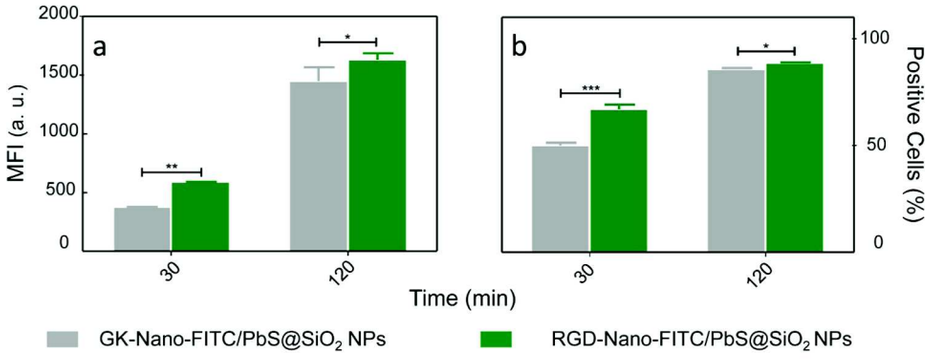

c

Incubation Time	30 (minutes)		120 (minutes)	
	MFI (a. u.)	Positive Cells (%)	MFI (a. u.)	Positive Cells (%)
GK-Nano-FITC/PbS@SiO_2 NPs	376 ± 2	50.2 ± 1.3	1450 ± 120	85.7 ± 0.6
RGD-Nano-FITC/PbS@SiO_2 NPs	591 ± 1	67.1 ± 2.0	1630 ± 50	88.7 ± 0.2

Figure 10. (a) Mean fluorescence intensity (MFI) and (b) percentage of positive cells obtained from a distribution of 10 000 cells in flow cytometry after WM266 cell incubation with GK-Nano-FITC/PbS QD@SiO_2 NP or RGD-Nano-FITC/PbS QD SiO_2 NP conjugates for 30 and 120 min at a peptide concentration of 100 nM. Control: untreated cells. Statistical significance calculated by a two-way analysis of variance (ANOVA) and the Bonferroni post hoc tests (GraphPad Prism vers. 5). Data indicated with * $p < 0.05$ and *** $p < 0.001$. (c) Table of mean PL intensity and of positive cell percentage at 30 and 120 min for WM266 cells incubated with GK-Nano-FITC/PbS QD@SiO_2 NP or RGD-Nano-FITC/PbS QD@SiO_2 NP conjugates.

corresponding reference nanosystems, characterized by the same chemical composition, optical and structural features, just without the RGD motif, to investigate the actual ability of the RGD sequence for selective cellular targeting.

3.3. In Vitro Investigation of the RGD-Nano-FITC Conjugated PbS QD@SiO_2 Nanoparticles on Cellular Uptake. An in vitro toxicity study was carried out to evaluate the viability of human malignant melanoma cells, WM266 cells, after their long-term exposure to the GK-Nano-FITC/PbS QD@SiO_2 NP and RGD-Nano-FITC/PbS QD@SiO_2 NP conjugates. WM266 cells, characterized by a predominant mutation in the BRAF gene occurring in 48% of metastatic melanomas,[54] were selected as they had been previously thoroughly characterized for the presence of high levels of $\alpha v\beta 3$ integrin,[44] thus providing a well-established model of $\alpha v\beta 3$ integrin receptor-related studies. In particular, WM266 cells were incubated with GK-Nano-FITC/PbS@SiO_2 NP and RGD-Nano-FITC/PbS SiO_2 NP conjugates, at concentrations from 5.1 to 0.0108 μM in peptide (in terms of GK-Nano-FITC or RGD-Nano-FITC peptide) for 72 h. Subsequently, conventional MTT assay assessed the cell viability, which was found to be concentration dependent. IC_{50} values of 597(±2) nM and 594(±3) nM in terms of RGD-Nano-FITC and GK-Nano-FITC peptide concentration, respectively, (Figure S5, see Supporting Information) were determined. Hence, the RGD-Nano-FITC/PbS SiO_2 NPs and GK-Nano-FITC/PbS@SiO_2 NPs, characterized by their very similar chemical composition, negative charge, and average hydrodynamic diameters, exhibited very comparable concentration-dependent toxicities.

According to the results obtained from cytotoxicity assay, the quantitative evaluation of the cellular uptake of GK-Nano-FITC/PbS QD@SiO_2 NP and RGD-Nano-FITC/PbS QD SiO_2 NP conjugates in WM266 cells was performed by intracellular flow cytometry experiments at a peptide concentration of 100 nM, and both peptide conjugates, with and without the RGD motif, were found to not be cytotoxic (Figure 10). In particular, WM266 cells were preliminarily incubated with the GK-Nano-FITC/PbS QD@SiO_2 NP and RGD-Nano-FITC/PbS QD SiO_2 NP conjugates for two different time periods, namely, 30 and 120 min. Untreated cells were used as "unlabeled" controls.

Subsequently, a quantitative study was carried out by flow-cytometric analysis measuring the mean fluorescence intensity (MFI) and the percentage of luminescent NP-containing cells (positive cells) over the total amount of cells (10 000).

The histograms of the MFI and positive cell percentage reported in Figure 10 and obtained by intracellular flow-cytometric analysis clearly prove the effective cellular internalization of both the GK-Nano-FITC/PbS QD@SiO_2 NPs and RGD-Nano-FITC/PbS QD@SiO_2 NPs. Interestingly, in the first 30 min, the values of MFI and positive cell percentage recorded for $\alpha v\beta 3$ integrin receptor-targeted PbS QD@SiO_2 NPs are higher than those achieved for the nontargeted NPs (Figure 10c), thus indicating a more efficient uptake of the targeted NPs in the WM266 cells, characterized by the relevant surface overexpression of the specific receptor for the RGD sequence. Consequently, it is reasonable to infer that the enhanced uptake of the RGD-Nano-FITC/PbS QD@SiO_2 NPs in the WM266 cells, with respect to that of the GK-Nano-FITC/PbS QD@SiO_2 NPs, can be reasonably ascribed to a receptor-mediated endocytosis of the targeted NPs, although an enhanced permeation and retention (EPR-mediated) effect seems to occur concurrently. Indeed, the ability of the RGD peptide functionalized NPs to pass through the cell membrane both by passive diffusion and receptor-mediated endocytosis has already been reported.[53,55] Such an explanation is further supported by the MFI and the positive cell percentage values obtained for the nontargeted NPs, which can be explained only by assuming cellular uptake by passive diffusion. Conversely, the higher MFI and positive cell percentage values recorded for the targeted NPs in the WM266 cells, where significant overexpression of the $\alpha v\beta 3$ receptor was revealed, indicated the good selectivity of the RGD-Nano-FITC/PbS QD@SiO_2 NPs for the $\alpha v\beta 3$ integrin receptor. A difference, although not large, in the MFI and positive cell percentage values of the cells incubated with the GK-Nano-FITC/PbS QD@SiO_2 NPs and

DOI: 10.1021/acsami.7b14155
ACS Appl. Mater. Interfaces 2017, 9, 43113−43126

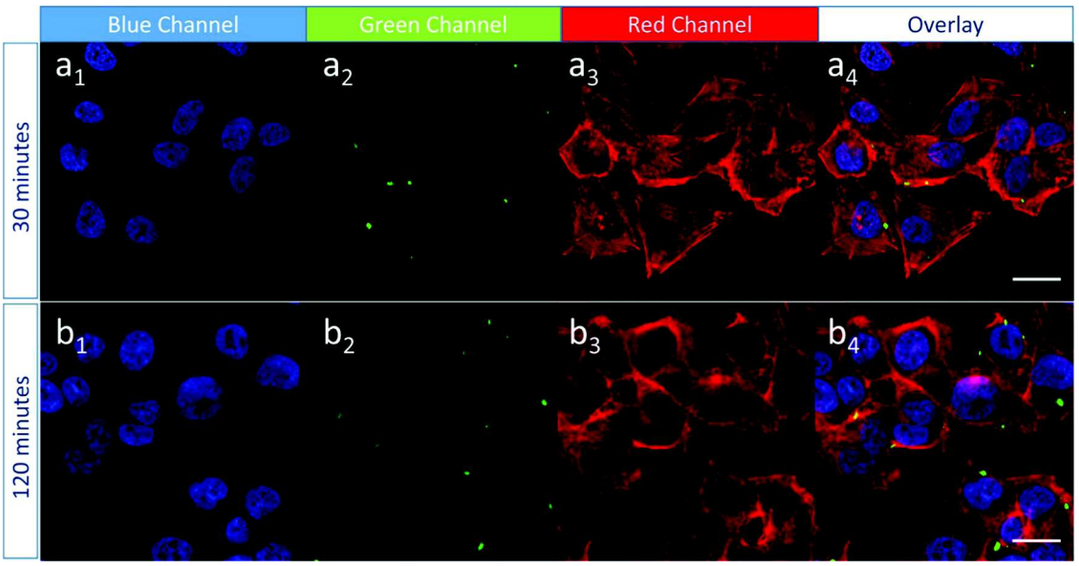

Figure 11. Confocal microscopy micrographs of fixed WM266 cells incubated for 30 or 120 min with RGD-Nano-FITC/PbS QD@SiO_2 NPs. (a1, b1) Blue channel, nuclei; (a2, b2) green channel, targeted NPs; (a3, b3) red channel, cytoskeleton; (a4, b4) overlay. Control: untreated cells. Scale bar 30 μm.

with the RGD-Nano-FITC/PbS QD SiO_2 NP conjugates, respectively, can still be observed in both cases after 120 min of cell treatment (Figure 10c). These results suggest that over a longer time, the cellular uptake of both the RGD-functionalized and the non RGD-functionalized NPs occurs mainly by passive diffusion, and in fact, the receptor-mediated endocytosis of the RGD-Nano-FITC/PbS QD@SiO_2 NP conjugates becomes a less dominant mechanism, probably due to the saturation of the $\alpha v\beta 3$ binding sites on the cellular membranes. Interestingly, the enhanced accumulation of the RGD-Nano-FITC/PbS QD@SiO_2 NPs in the cells at early times can really represent a useful advantage for their future in vivo application as nanoprobes able to perform integrin-targeted NIR optical imaging, because their in vivo blood half-life could be no longer than 120 min. Indeed, radio-labeled compounds functionalized with the cyclic RGD motif were found to be able to be quickly and highly internalized in tumor cells at early times, within the first 30 min after intravenous injection, before the occurrence of their elimination via metabolism, hepatobiliary or renal excretion, or blood clearance.[57] It has been well documented that the functionalization of NPs with the RGD sequence, instead of small molecules, as in vivo probes, increases the blood half-life, although it was also reported that the clearance process takes place in the first 120 minutes. For example, Jia et al. reported that RGD-modified Fe_3O_4 NPs were characterized by a blood half-life of about 90 min, which was much longer than that of small molecules based on clinical Gd complex or other iron oxide NPs.[58]

Finally, the effective in vitro ability of the RGD-Nano-FITC/PbS SiO_2 NP conjugates to be internalized in the WM266 cells was also demonstrated by means of confocal microscopy investigation (Figure 11).

The cells were incubated with the RGD-Nano-FITC/PbS QD@SiO_2 NPs at a peptide concentration of 400 nM for 30 (Figure 11, panels a1−a4) and 120 min (Figure 11, panels b1−b4) and, after the fixation process, they were stained with DAPI and Phalloidin-TRIC for the visualization of the nuclei and F-actin cytoskeleton of the cells, respectively. The a1, a2, and a3 panels and b1, b2, and b3 panels of Figure 11 show the individual blue, green, and red PL of DAPI, RGD-Nano-FITC/PbS QD@SiO_2 NPs, and Phalloidin-TRIC, respectively, in fixed WM266 cells. From the panels a4 and b4, the association between the blue, green, and red channel can be observed. The cellular imaging experiments clearly proved the ability of the RGD-Nano-FITC/PbS QD@SiO_2 NPs to be internalized by cells and the dependence of the cellular uptake on the incubation time. In particular, the green spots evident already after 30 min in the micrographs, and ascribed to the emission from the FITC dye, present in the prepared nanostructures, indicate that the targeted conjugates accumulated inside cells already at the investigated short time period (Figure 11, panels a1−a4). Indeed, an enhanced green emission was detected when the cells were exposed to the conjugates for the longer tested incubation time, although not all cells were able to internalize the RGD-Nano-FITC/PbS QD@SiO_2 NPs after 120 min (Figure 11, panels b1−b4). Remarkably, a perfect agreement with the results of the flow cytometry analysis was found (Figure 10).

4. CONCLUSIONS

NIR emitting silica-coated PbS QDs, synthesized by carefully controlling their size, shape, and surface charge and conjugated with a designed RGD-based peptide, were proposed as targeting, single nanoparticle systems for optical imaging, thanks to their ability to combine the selectivity of the peptide toward integrin $\alpha v\beta 3$ with the photostability and emission properties of the inorganic QDs.

In particular, PbS SiO_2 NPs, conjugated with the green fluorescent RGD-Nano-FITC peptide were obtained, along with the analogous fluorescent system without the RGD motif, which is GK-Nano-FITC and was used as the control system. The selective targeting ability of the RGD sequence conjugated NPs toward the $\alpha v\beta 3$ integrin was evaluated.

Complementary optical and structural investigation of the NP bioconjugation process demonstrated the good colloidal stability of the resulting structures, highlighting how the NIR

DOI: 10.1021/acsami.7b14155
ACS Appl. Mater. Interfaces 2017, 9, 43113−43126

emitting characteristic was fully preserved in an aqueous environment and also upon bioconjugation with the peptides.

The silica-coated PbS QDs conjugated with RGD peptide were found, with in vitro investigation by confocal microscopy, to be internalized in the WM266 cells, and, the flow-cytometric studies demonstrated the bioconjugated NP selectivity for the $\alpha v\beta 3$ integrin receptor mainly within the first 30 min, when receptor-mediated endocytosis seems to dominate the passive diffusion of NPs in the WM266 cells. The RGD peptide-conjugated PbS QD@SiO_2 NPs represent, therefore, a highly promising nanoprobe, with an architecture suitably designed not only to preserve their relevant emission in the NIR region, but also to accomplish cellular targeting toward integrin receptors, thus opening an avenue for potential application for NIR bioimaging and imaging-guided surgery.

■ ASSOCIATED CONTENT

Supporting Information

The Supporting Information is available free of charge on the ACS Publications website at DOI: 10.1021/acsami.7b14155.

Systematic study on the effects of silica shell growth parameters, namely, PbS QD concentration and silica precursor molar ratio, on the size, morphology, and optical properties of the resulting silica-coated PbS QDs, starting from PbS QDs of 2.4 and 2.6 nm; vis−NIR absorption spectrum of PbS@SiO_2 NPs dispersed in ethanol obtained starting from OLEA/TOP capped PbS QDs with an average diameter of 2.6 nm; quantum yield evaluation of functionalized PbS QDs; PL investigation performed on a mixture containing amine-functionalized silica-coated PbS QDs and the free RGD-Nano-FITC peptide, after their incubation without any linker, to prove the formation of a covalent bond between the amine groups grafted on silica-coated PbS QDs and the amine group introduced into the peptide structure; cell viability profiles, by MTT assay, of WM266 cells incubated with RGD-Nano-FITC/PbS QD@SiO_2 NPs or GK- Nano-FITC/PbS QD@SiO_2 NPs for 72 h (PDF)

■ AUTHOR INFORMATION

Corresponding Authors

*E-mail: n.depalo@ba.ipcf.cnr.it (N.D.).
*E-mail: lucia.curri@ba.ipcf.cnr.it (M.L.C.).

ORCID

N. Depalo: 0000-0002-2107-2762
N. Denora: 0000-0002-7756-7828
M. Saviano: 0000-0001-5086-2459
L. Zaccaro: 0000-0001-6843-0152

Present Address

[V]Electron Microscopy Facility, Istituto Italiano di Tecnologia (IIT), via Morego 30, Genova, Italy (D.D.).

Author Contributions

[O]N.D. and M.C. are the co-first authors.

Author Contributions

Design, preparation, and characterization of luminescent silica-coated nanostructures conjugated with cyclic RGD peptide; coordination and supervision of the different multidisciplinary experimental contributions, from the preparation and bioconjugation of the nanoparticles up to in vitro tests; conception of the work; analysis of the overall results; substantial contribution in the drafting of the manuscript were done by N.D. M.C. designed, synthesized, and characterized luminescent silica-coated nanoparticles; discussed the results; and substantially contributed to the drafting of the manuscript. I.D.P. was responsible for peptide synthesis and labeling. G.V. conducted cellular uptake studies by confocal microscopy and drafted the manuscript. R.M.I. performed cytotoxicity assay and cellular uptake experiments of the peptide conjugates. E.A. conducted cellular uptake studies by confocal microscopy and cytofluorimetic analysis. D.D. was responsible for the synthesis and bioconjugation of luminescent silica-coated nanoparticles. D.C. performed peptide characterization. E.F. conducted morphological characterization of the nanostructures by TEM analysis at each functionalization step. N.D. performed the cytotoxicity and cellular uptake studies on the peptide conjugates and critical discussion on their biological behavior. V.L. characterized the prepared nanostructures at each functionalization step by DLS analysis and performed ζ-potential measurements. Critical discussion on cellular uptake studies by cytofluorimetic analysis was conducted by F.M. M.S. designed peptides. Critical discussion on the overall results was conducted by A.A. M.S. contributed to manuscript revision through critical discussion of the results. A.D.G. performed purification and characterization of peptides. L.Z. was responsible for the design and experiments concerning the synthesis, purification, and characterization of peptide and critical discussion of the results. M.L.C. was involved in the conception and supervision of the work and coordination of the activities, critical discussion on the overall results, and substantial contribution to drafting and revising the manuscript.

Notes

The authors declare no competing financial interest.

■ ACKNOWLEDGMENTS

The work has been partially supported by Nanomax-Integrable sensors for pathological biomarkers diagnosis (N-CHEM), National Sens&Micro LAB (POFESR 2007−2013), NANO-fotocatalizzatori per un'Atmosfera più PULita (NANOAPULIA), PONa300369 (Laboratorio Sistema), and by the National PRIN 2012 Prot. 20128ZZS2H and Prot. 2012T9XHH7 projects.

■ REFERENCES

(1) Zhang, L.; Bhatnagar, S.; Deschenes, E.; Thurber, G. M. Mechanistic and quantitative insight into cell surface targeted molecular imaging agent design. *Sci. Rep.* **2016**, *6*, No. 25424.

(2) Sun, X.; Li, Y.; Liu, T.; Li, Z.; Zhang, X.; Chen, X. Peptide-based imaging agents for cancer detection. *Adv. Drug Delivery Rev.* **2017**, *110−111*, 38−51.

(3) Juhl, K.; Christensen, A.; Persson, M.; Ploug, M.; Kjaer, A. Peptide-Based Optical uPAR Imaging for Surgery: In Vivo Testing of ICG-Glu-Glu-AE105. *PLoS One* **2016**, *11*, No. e0147428.

(4) Fernández, A.; Vendrell, M. Smart fluorescent probes for imaging macrophage activity. *Chem. Soc. Rev.* **2016**, *45*, 1182−1196.

(5) Reubi, J. C.; Maecke, H. R. Peptide-based probes for cancer imaging. *J. Nucl. Med.* **2008**, *49*, 1735−1738.

(6) Okarvi, S. M. Peptide-based radiopharmaceuticals: future tools for diagnostic imaging of cancers and other diseases. *Med. Res. Rev.* **2004**, *24*, 357−397.

(7) Stoykow, C.; Erbes, T.; Maecke, H. R.; Bulla, S.; Bartholomä, M.; Mayer, S.; Drendel, V.; Bronsert, P.; Werner, M.; Gitsch, G.; Weber, W. A.; Stickeler, E.; Meyer, P. T. Gastrin-releasing Peptide Receptor Imaging in Breast Cancer Using the Receptor Antagonist ^{68}Ga-RM2 And PET. *Theranostics* **2016**, *6*, 1641−1650.

DOI: 10.1021/acsami.7b14155
ACS Appl. Mater. Interfaces 2017, 9, 43113−43126

(8) Morgat, C.; Mishra, A. K.; Varshney, R.; Allard, M.; Fernandez, P.; Hindié, E. Targeting Neuropeptide Receptors for Cancer Imaging and Therapy: Perspectives with Bombesin, Neurotensin, and Neuropeptide-Y Receptors. *J. Nucl. Med.* **2014**, *55*, 1650−1657.
(9) Tang, B.; Yong, X.; Xie, R.; Li, Q.-W.; Yang, S.-M. Vasoactive intestinal peptide receptor-based imaging and treatment of tumors. *Int. J. Oncol.* **2014**, *44*, 1023−1031.
(10) Cai, W.; Niu, G.; Chen, X. Imaging of integrins as biomarkers for tumor angiogenesis. *Curr. Pharm. Des.* **2008**, *14*, 2943−2973.
(11) Reubi, J. C. Targeting CCK receptors in human cancers. *Curr. Top. Med. Chem.* **2007**, *7*, 1239−1242.
(12) Körner, M.; Stockli, M.; Waser, B.; Reubi, J. C. GLP-1 receptor expression in human tumors and human normal tissues: potential for in vivo targeting. *J. Nucl. Med.* **2007**, *48*, 736−743.
(13) Miao, Y.; Quinn, T. P. Alpha-melanocyte stimulating hormone peptide-targeted melanoma imaging. *Front Biosci.* **2007**, *12*, 4514−4524.
(14) Deutscher, S. L. Phage display in molecular imaging and diagnosis of cancer. *Chem. Rev.* **2010**, *110*, 3196−3211.
(15) Li, Z. J.; Cho, C. H. Development of peptides as potential drugs for cancer therapy. *Curr. Pharm. Des.* **2010**, *16*, 1180−1189.
(16) Lee, S.; Xie, J.; Chen, X. Peptide-based probes for targeted molecular imaging. *Biochemistry* **2010**, *49*, 1364−1376.
(17) Fani, M.; Maecke, H. R.; Okarvi, S. M. Radiolabeled Peptides: Valuable Tools for the Detection and Treatment of Cancer. *Theranostics* **2012**, *2*, 481−501.
(18) Zhu, D.; Qin, Y.; Wang, J.; Zhang, L.; Zou, S.; Zhu, X.; Zhu, L. Novel Glypican-3-Binding Peptide for in Vivo Hepatocellular Carcinoma Fluorescent Imaging. *Bioconjugate Chem.* **2016**, *27*, 831−839.
(19) Maschauer, S.; Einsiedel, J.; Hübner, H.; Gmeiner, P.; Prante, O. (18)F- and (68)Ga-Labeled Neurotensin Peptides for PET Imaging of Neurotensin Receptor 1. *J. Med. Chem.* **2016**, *59*, 6480−6492.
(20) Li, L.; Wu, Y.; Wang, Z.; Jia, B.; Hu, Z.; Dong, C.; Wang, F. SPECT/CT Imaging of the Novel HER2-Targeted Peptide Probe ^{99m}Tc-HYNIC-H6F in Breast Cancer Mouse Models. *J. Nucl. Med.* **2017**, *58*, 821−826.
(21) Preslar, A. T.; Tantakitti, F.; Park, K.; Zhang, S.; Stupp, S. I.; Meade, T. J. ^{19}F Magnetic Resonance Imaging Signals from Peptide Amphiphile Nanostructures Are Strongly Affected by Their Shape. *ACS Nano* **2016**, *10*, 7376−7384.
(22) Valente, G.; Depalo, N.; de Paola, I.; Iacobazzi, R. M.; Denora, N.; Laquintana, V.; Comparelli, R.; Altamura, E.; Latronico, T.; Altomare, M.; Fanizza, E.; Striccoli, M.; Agostiano, A.; Saviano, M.; Del Gatto, A.; Zaccaro, L.; Curri, M. L. Integrin-targeting with peptide-bioconjugated semiconductor-magnetic nanocrystalline heterostructures. *Nano Res.* **2016**, *9*, 644−662.
(23) Escobedo, J. O.; Rusin, O.; Lim, S.; Strongin, R. M. NIR dyes for bioimaging applications. *Curr. Opin. Chem. Biol.* **2010**, *14*, 64−70.
(24) Bouccara, S.; Sitbon, G.; Fragola, A.; Loriette, V.; Lequeux, N.; Pons, T. Enhancing fluorescence in vivo imaging using inorganic nanoprobes. *Curr. Opin. Biotechnol.* **2015**, *34*, 65−72.
(25) Depalo, N.; De Leo, V.; Corricelli, M.; Gristina, R.; Valente, G.; Casamassima, E.; Comparelli, R.; Laquintana, V.; Denora, N.; Fanizza, E.; Striccoli, M.; Agostiano, A.; Catucci, L.; Curri, M. L. Lipid-based systems loaded with PbS nanocrystals: near infrared emitting trackable nanovectors. *J. Mater. Chem. B* **2017**, *5*, 1471−1481.
(26) Corricelli, M.; Depalo, N.; Di Carlo, E.; Fanizza, E.; Laquintana, V.; Denora, N.; Agostiano, A.; Striccoli, M.; Curri, M. L. Biotin-decorated silica coated PbS nanocrystals emitting in the second biological near infrared window for bioimaging. *Nanoscale* **2014**, *6*, 7924−7933.
(27) Kim, D.; Lee, N.; Park, Y.; Hyeon, T. Recent Advances in Inorganic Nanoparticle-Based NIR Luminescence Imaging: Semiconductor Nanoparticles and Lanthanide Nanoparticles. *Bioconjugate Chem.* **2017**, *28*, 115−123.
(28) Fanizza, E.; Urso, C.; Iacobazzi, R. M.; Depalo, N.; Corricelli, M.; Panniello, A.; Agostiano, A.; Denora, N.; Laquintana, V.; Striccoli, M.; Curri, M. L. Fabrication of Photoactive Heterostructures based on Quantum Dots Decorated with Au Nanoparticles. *Sci. Technol. Adv. Mater.* **2016**, *17*, 98−108.
(29) Fanizza, E.; Iacobazzi, R. M.; Laquintana, V.; Valente, G.; Caliandro, G.; Striccoli, M.; Agostiano, A.; Cutrignelli, A.; Lopedota, A.; Curri, M. L.; Franco, M.; Depalo, N.; Denora, N. Highly selective luminescent nanostructures for mitochondrial imaging and targeting. *Nanoscale* **2016**, *8*, 3350−3361.
(30) Bilan, R.; Fleury, F.; Nabiev, I.; Sukhanova, A. Quantum Dot Surface Chemistry and Functionalization for Cell Targeting and Imaging. *Bioconjugate Chem.* **2015**, *26*, 609−624.
(31) Wang, L. W.; Peng, C. W.; Chen, C.; Li, Y. Quantum dots-based tissue and in vivo imaging in breast cancer researches: current status and future perspectives. *Breast Cancer Res. Treat.* **2015**, *151*, 7−17.
(32) Alibolandi, M.; Abnous, K.; Sadeghi, F.; Hosseinkhani, H.; Ramezani, M.; Hadizadeh, F. Folate receptor-targeted multimodal polymersomes for delivery of quantum dots and doxorubicin to breast adenocarcinoma: *In vitro* and in vivo evaluation. *Int. J. Pharm.* **2016**, *500*, 162−178.
(33) Latronico, T.; Depalo, N.; Valente, G.; Fanizza, E.; Laquintana, V.; Denora, N.; Fasano, A.; Striccoli, M.; Colella, M.; Agostiano, A.; Curri, M. L.; Liuzzi, G. M. Cytotoxicity Study on Luminescent Nanocrystals Containing Phospholipid Micelles in Primary Cultures of Rat Astrocytes. *PLoS One* **2016**, *11*, No. e0153451.
(34) Bilan, R.; Nabiev, I.; Sukhanova, A. Quantum Dot-Based Nanotools for Bioimaging, Diagnostics, and Drug Delivery. *ChemBioChem* **2016**, *17*, 2103−2114.
(35) Cai, W.; Chen, X. Nanoplatforms for targeted molecular imaging in living subjects. *Small* **2007**, *3*, 1840−1854.
(36) Smith, A. M.; Duan, H.; Mohs, A. M.; Nie, S. Bioconjugated quantum dots for in vivo molecular and cellular imaging. *Adv. Drug Delivery Rev.* **2008**, *60*, 1226−1240.
(37) Wang, Z.; Chui, W. K.; Ho, P. C. Integrin targeted drug and gene delivery. *Expert Opin. Drug Delivery* **2010**, *7*, 159−171.
(38) Zhang, Y.; Yang, Y.; Cai, W. Multimodality Imaging of Integrin $\alpha v\beta 3$ Expression. *Theranostics* **2011**, *1*, 135−148.
(39) Choi, N.; Kim, S.-M.; Hong, K. S.; Cho, G.; Cho, J.-H.; Lee, C.; Ryu, E. K. The use of the fusion protein RGD-HSA-TIMP2 as a tumor targeting imaging probe for SPECT and PET. *Biomaterials* **2011**, *32*, 7151−7158.
(40) Danhier, F.; Le Breton, A.; Préat, V. RGD-Based Strategies To Target Alpha(v) Beta(3) Integrin in Cancer Therapy and Diagnosis. *Mol. Pharmaceutics* **2012**, *9*, 2961−2973.
(41) Ma, Y.; Ai, G.; Zhang, C.; Zhao, M.; Dong, X.; Han, Z.; Wang, Z.; Zhang, M.; Liu, Y.; Gao, W.; Li, S.; Gu, Y. Novel Linear Peptides with High Affinity to $\alpha v\beta 3$ Integrin for Precise Tumor Identification. *Theranostics* **2017**, *7*, 1511−1523.
(42) Zannetti, A.; Del Vecchio, S.; Iommelli, F.; Del Gatto, A.; De Luca, S.; Zaccaro, L.; Papaccioli, A.; Sommella, J.; Panico, M.; Speranza, A.; Grieco, P.; Novellino, E.; Saviano, M.; Pedone, C.; Salvatore, M. Imaging of$\alpha v\beta_3$Expression by a Bifunctional Chimeric RGD Peptidenot Cross-Reacting with$\alpha v\beta_5$. *Clin. Cancer Res.* **2009**, *15*, 5224−5233.
(43) Arosio, D.; Manzoni, L.; Araldi, E. M. V.; Scolastico, C. Cyclic RGD Functionalized Gold Nanoparticles for Tumor Targeting. *Bioconjugate Chem.* **2011**, *22*, 664−672.
(44) Farina, B.; de Paola, I.; Russo, L.; Capasso, D.; Liguoro, A.; Del Gatto, A.; Saviano, M.; Pedone, P. V.; Di Gaetano, S.; Malgieri, G.; Zaccaro, L.; Fattorusso, R. A Combined NMR and Computational Approach to Determine the RGDechi-hCit-α v β 3 Integrin Recognition Mode in Isolated Cell Membranes. *Chem. − Eur. J.* **2016**, *22*, 681−693.
(45) Corricelli, M.; Enrichi, F.; Altamura, D.; De Caro, L.; Giannini, C.; Falqui, A.; Agostiano, A.; Curri, M. L.; Striccoli, M. Near infrared emission from monomodal and bimodal PbS nanocrystal superlattices. *J. Phys. Chem. C* **2012**, *116*, 6143−6152.
(46) Fanizza, E.; Depalo, N.; Clary, L.; Agostiano, A.; Striccoli, M.; Curri, M. L. A combined size sorting strategy for monodisperse plasmonic nanostructures. *Nanoscale* **2013**, *5*, 3272−3282.

DOI: 10.1021/acsami.7b14155
ACS Appl. Mater. Interfaces 2017, 9, 43113−43126

(47) Fanizza, E.; Urso, C.; Pinto, V.; Cardone, A.; Ragni, R.; Depalo, N.; Curri, M. L.; Agostiano, A.; Farinola, G. M.; Striccoli, M. Single white light emitting hybrid nanoarchitectures based on functionalized quantum dots. *J. Mater. Chem. C* **2014**, *2*, 5286−5291.
(48) Fanizza, E.; Depalo, N.; Clary, L.; Agostiano, A.; Striccoli, M.; Curri, M. L. A combined size sorting strategy for monodisperse plasmonic nanostructures. *Nanoscale* **2013**, *5*, 3272−3282.
(49) Depalo, N.; Iacobazzi, R. M.; Valente, G.; Arduino, I.; Villa, S.; Canepa, F.; Laquintana, V.; Fanizza, E.; Striccoli, M.; Cutrignelli, A.; Lopedota, A.; Porcelli, L.; Azzariti, A.; Franco, M.; Curri, M. L.; Denora, N. Sorafenib delivery nanoplatform based on superparamagnetic iron oxide nanoparticles magnetically targets hepatocellular carcinoma. *Nano Res.* **2017**, *10*, 2431−2448.
(50) Scarì, G.; Porta, F.; Fascio, U.; Avvakumova, S.; Dal Santo, V.; De Simone, M.; Saviano, M.; Leone, M.; Del Gatto, A.; Pedone, C.; Zaccaro, L. Gold Nanoparticles Capped by a GC-Containing Peptide Functionalized with an RGD Motif for Integrin Targeting. *Bioconjugate Chem.* **2012**, *23*, 340−349.
(51) Krpetić, Z.; Nativo, P.; Porta, F.; Brust, M. A multidentate peptide for stabilization and facile bioconjugation of gold nanoparticles. *Bioconjugate Chem.* **2009**, *20*, 619−624.
(52) Porta, F.; Speranza, G.; Krpetić, Ž.; Dal Santo, V.; Francescato, P.; Scarì, G. Gold nanoparticles capped by peptides. *Mater. Sci. Eng., B* **2007**, *140*, 187−194.
(53) Shuhendler, A. J.; Prasad, P.; Leung, M.; Rauth, A. M.; Da Costa, R. S.; Wu, X. Y. A Novel Solid Lipid Nanoparticle Formulation for Active Targeting to Tumor $\alpha v\beta 3$ Integrin Receptors Reveals Cyclic RGD as A Double-Edged Sword. *Adv. Healthcare Mater.* **2012**, *1*, 600−608.
(54) Gentilcore, G.; Madonna, G.; Mozzillo, N.; Ribas, A.; Cossu, A.; Palmieri, G.; Ascierto, P. A. Effect of dabrafenib on melanoma cell lines harbouring the BRAF $V^{600D/R}$ mutations. *BMC Cancer* **2013**, *13*, 17.
(55) Capasso, D.; de Paola, I.; Liguoro, A.; Del Gatto, A.; Di Gaetano, S.; Guarnieri, D.; Saviano, M.; Zaccaro, L. RGDechi-hCit: $\alpha v\beta 3$ selective pro-apoptotic peptide as potential carrier for drug delivery into melanoma metastatic cells. *PLoS One* **2014**, *9*, No. e106441.
(56) Laquintana, V.; Denora, N.; Lopalco, A.; Lopedota, A.; Cutrignelli, A.; Lasorsa, F. M.; Agostino, G.; Franco, M. Translocator protein ligand-PLGA conjugated nanoparticles for 5-fluorouracil delivery to glioma cancer cells. *Mol. Pharmaceutics* **2014**, *11*, 859−871.
(57) Lim, E. H.; Danthi, N.; Bednarski, M.; Li, K. C. P. A review: Integrin $\alpha v\beta 3$-targeted molecular imaging and therapy in angiogenesis. *Nanomed.: Nanotechnol., Biol., Med.* **2005**, *1*, 110−114.
(58) Jia, Z.; Song, L.; Zang, F.; Song, J.; Zhang, W.; Yan, C.; Xie, J.; Ma, Z.; Ma, M.; Teng, G.; Gu, N.; Zhang, Y. Active-target T1-weighted MR Imaging of Tiny Hepatic Tumor via RGD Modified Ultra-small Fe_3O_4 Nanoprobes. *Theranostics* **2016**, *6*, 1780−1791.

DOI: 10.1021/acsami.7b14155
ACS Appl. Mater. Interfaces 2017, 9, 43113−43126